Clinical Assessment of Mirror Artifacts in Spectral-Domain Optical Coherence Tomography

Joseph Ho,[1,2] *Dinorah P. E. Castro,*[1] *Leonardo C. Castro,*[1] *Yueli Chen,*[3] *Jonathan Liu,*[3] *Cynthia Mattox,*[1] *Chandrasekharan Krishnan,*[1] *James G. Fujimoto,*[3] *Joel S. Schuman,*[4] *and Jay S. Duker*[1]

Purpose. To investigate the characteristics of a spectral-domain optical coherence tomography (SD-OCT) image phenomenon known as the mirror artifact, calculate its prevalence, analyze potential risk factors, measure severity, and correlate it to spherical equivalent and central visual acuity (VA).

Methods. OCT macular cube 512 × 128 scans taken between January 2008 and February 2009 at the New England Eye Center were analyzed for the presence of mirror artifacts. Artifact severity was determined by the degree of segmentation breakdown that it caused on the macular map. A retrospective review was conducted of the medical records of patients with artifacts and of a random control group without artifacts.

Results. Of 1592 patients, 9.3% (148 patients, 200 eyes) had scans that contained mirror artifacts. A significantly more myopic spherical equivalent ($P < 0.001$), worse VA ($P < 0.001$), longer axial lengths ($P = 0.004$), and higher proportions of moderate to high myopia ($P < 0.001$) were found in patients with mirror artifacts than in patients without artifacts. Worse VA was associated with increased artifact severity ($P = 0.04$).

Conclusions. In all scans analyzed, a high prevalence of mirror artifacts was found. This image artifact was often associated with patients with moderate to high myopia. Improvements in instrumentation may be necessary to resolve this problem in moderately and highly myopic eyes. Operators should be advised to properly position the retina when scanning eyes. In cases in which peripheral abnormalities in topographic measurements of retinal thickness are found, corresponding OCT scans should be examined for the presence of mirror artifacts.

From the [1]New England Eye Center, Tufts Medical Center, Boston, Massachusetts; the [2]Boston University School of Medicine, Boston, Massachusetts; the [3]Department of Electrical Engineering and Computer Science and Research Laboratory of Electronics, Massachusetts Institute of Technology, Cambridge, Massachusetts; and the [4]University of Pittsburgh Medical Center Eye Center, Eye and Ear Institute, Pittsburgh, Pennsylvania.

Supported in part by a Research to Prevent Blindness Challenge grant to the New England Eye Center/Department of Ophthalmology, Tufts University School of Medicine; National Institutes of Health Grants R01-EY11289–23, R01-EY13178-09, and R01-EY013516-16; and Air Force Office of Scientific Research Grants FA9550-07-1-0101 and FA9550-07-1-0014.

Submitted for publication May 29, 2009; revised December 3, 2009; accepted February 2, 2010.

Disclosure: **J. Ho**, Optovue, Inc. (R); **D.P.E. Castro**, None; **L.C. Castro**, Optovue, Inc. (R); **Y. Chen**, None; **J. Liu**, None; **C. Mattox**, None; **C. Krishnan**, None; **J.G. Fujimoto**, Optovue, Inc. (I), P; **J.S. Schuman**, Carl Zeiss Meditec, Inc. (F, R), Optovue, Inc. (R), P; **J.S. Duker**, Carl Zeiss Meditec, Inc. (F), Optovue, Inc. (F), Topcon Medical Systems, Inc. (F)

Corresponding author: Jay S. Duker, Department of Ophthalmology, Tufts Medical Center, 800 Washington Street, Box 450, Boston, MA, 02111; jduker@tuftsmedicalcenter.org.

(*Invest Ophthalmol Vis Sci.* 2010;51:3714–3720) DOI:10.1167/iovs.09-4057

Optical coherence tomography[1] (OCT) is a device designed to provide high-quality cross-sectional images of biological tissues. Since its introduction, it has become an invaluable ancillary tool for ophthalmologists for the diagnosis and treatment of retinal diseases and glaucoma.

With the advent of Fourier domain OCT detection, OCT scanning speed has increased more than 100-fold, from 400 A-scans/s to a maximum of approximately 300,000 A-scans/s.[2,3] Fourier-domain OCT detection is performed in two ways: spectral-domain (SD) OCT with a spectrometer and a line scan camera or swept-source OCT with a rapidly tunable laser source.[4] In addition to improvements to OCT imaging speed, the increase in the bandwidth of the light source used has led to an improvement in axial resolution from 10 μm to as high as 2 to 5 μm.[4,5] Typical commercial instruments have resolutions of 5 to 7 μm and imaging speeds of 25,000 to 50,000 A-scans/s. The improved resolution combined with the dense scan patterns and reduced motion artifacts due to higher scanning speeds give ophthalmologists a more accurate depiction of true retina topography and anatomy than is possible with time-domain detection. The increase in data obtainable promises to enable more accurate quantitative analysis, which is becoming important in the evaluation of new treatments for macular diseases.[6] Quantitative analysis of retinal thickness typically involves measuring the full retinal thickness in each subfield of the nine-quadrant Early Diagnosis and Treatment Diabetic Retinopathy (EDTRS) map.[7] This analysis relies on correct automatic placement of the inner and outer retinal segmentation lines. Several image artifacts can occur during acquisition or processing of OCT scans, preventing accurate segmentation. Given the potential implications that segmentation errors have on quantitative OCT analysis, artifact analysis has become an important area of recent research. Several causes of artifacts common to OCT scans have been described in the literature, including software algorithm breakdown,[8–12] eccentric fixation,[8] and out-of-range artifacts[8] (in which OCT scans are moved out of the scanning range).

Mirror artifacts arise from the Fourier transformation used in OCT systems with Fourier-domain detection, including SD and swept-source OCT. Fourier-domain detection cannot distinguish positive from negative time delays and therefore produce OCT images that are symmetrical around the 0-delay line (Fig. 1A). In addition, there is a sensitivity roll-off in Fourier-domain instruments, in which sensitivity decreases with increased distance from the 0-delay line. This decrease in sensitivity occurs because the spectrometer has limited resolution, and reflections farther away from the 0 delay produce finer interference signals. This sensitivity roll-off can be seen in Figure 1 as a variation in the intensity of the RPE layer, which

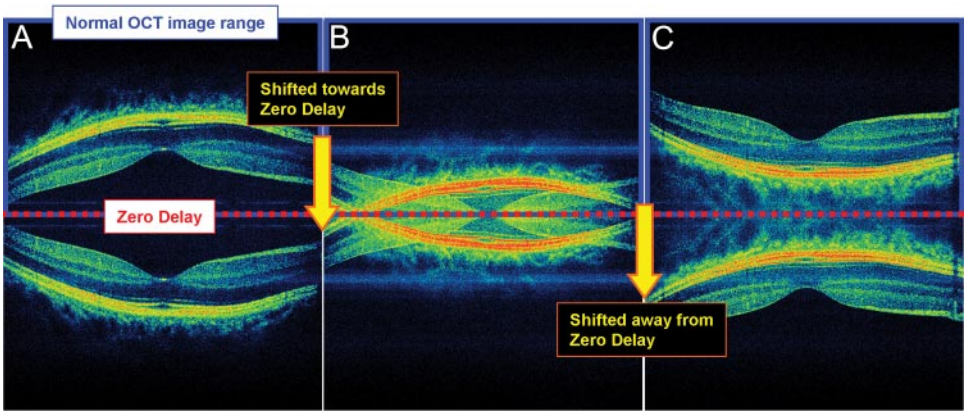

FIGURE 1. Explanation of the generation of mirror artifacts. A prototype, 3-μm, high speed, ultrahigh-resolution SD-OCT was used for acquisition of all images. (**A**) SD-OCT image is normally symmetrical about the 0-delay line after Fourier transformation. The lower half of the image is normally removed during image processing; thus, only the top half of the image appears. The inner retina of both portions of the symmetric image is closer to the 0-delay line than is the choroid. (**B**) OCT scan image is artificially moved toward the 0-delay line. When part of the visible image crosses the line, the other half of the symmetric image (normally unseen) simultaneously crosses into the visible half of the scan box. Thus, the visible half of the OCT scan now contains the normally visible part of the OCT scan that has not crossed the 0-delay line, along with the portion of the normally unseen OCT scan that has crossed the line. (**C**) The OCT image continues to be moved toward the 0-delay line until the entire portion of the normally visible half of the symmetric image crosses the line. Now, the normally visible half is no longer visible, and the normally unseen half is visible. The choroid in both halves of the symmetric image is closer to the 0-delay line than is the inner retina.

appears brightest when it is near 0 delay (Fig. 1C) and weakest when it is farther from it (Fig. 1A). Most commercial instruments are designed to work with the retina placed posterior to the 0-delay line (Fig. 1A), to enhance sensitivity for imaging epiretinal membranes or vitreal detachments. Finally, instruments have a maximum axial scan depth range over which imaging can be performed.

Before displaying the OCT scans, commercial instruments truncate one side of the OCT image, leaving the remaining half for image display. This method works when the retina is contained solely on one side of the 0-delay position. However, when the retinal image crosses the 0-delay line, the symmetric mirror image on the truncated side crosses into the scanning range on the displayed portion of the OCT image (Fig. 1B). Thus, the OCT image appears to be folded onto itself, sometimes extending past the retina and into the choroid. This phenomenon is known as a mirror artifact. Since the maximum sensitivity occurs when the instrument is adjusted with the retina near the 0 delay and there is a limited axial scan depth range, measurements are performed with the retina near the 0 delay. Thus, mirror artifacts can result from axial eye movement during imaging.

The mirror artifact and methods of mitigating it have been described in the engineering literature,[13–23] but have not yet been evaluated and elucidated in a clinical context. These methods include phase shifting or modulation methods[20,21,23] and frequency-shifting methods[22] to shift the 0-delay line. Mirror artifacts can result in errors in interpretation as well as quantitation. The purpose of this study was to investigate the effect of the OCT mirror artifact in a clinical context. The prevalence of its occurrence was calculated, the predisposing factors for it were examined, and its effects on accurate segmentation were evaluated.

METHODS

Subjects and OCT Scan Protocol

A retrospective review was conducted of Cirrus HD-OCT (software version 3.0; Carl Zeiss Meditec, Inc., Dublin, CA) scans. The Cirrus OCT has an axial image resolution of 5 μm, an imaging speed of 27,000 A-scans/s and an axial scan depth range of 2 mm, with 1024 pixels. Imaging was performed with the macular cube protocol, consisting of 512 × 128 scans acquired in 1.3 seconds on 1592 patients attending the retina, glaucoma, and neuro-ophthalmology clinics at the New England Eye Center, Tufts Medical Center, between January 2008 and February 2009. This study was approved by the Tufts Medical Center Institutional Review Board and was conducted in accordance with the ethics stated in the 1964 Declaration of Helsinki.

OCT Image Analysis

All 128 horizontal OCT B-scans acquired in the macular cube 512 × 128 protocol were examined by one evaluator (JH) for the presence of mirror artifacts, defined as the visible reflection or flipping of the retina down toward the choroid region Fig. 2A). In cases in which the mirror artifact did not cause reflection all the way into the choroid, a second evaluator (LCC) graded the scan individually, and disagreements occurring between the two graders were adjudicated after those scans were viewed together and carefully discussed. In addition, artifact severity was determined via the three-dimensional topographic macular map. Mirror artifacts cause segmentation breakdown, where the inner and outer retinal segmentation lines overlap each other generating various numbers of crescent-shaped defects at the corners and borders of the topographic map. Thus, artifact severity was measured by dividing the topographic map into five regions and counting the number of regions containing mirror artifacts (Fig. 2A, right).

Chart Review, Mirror Artifacts

Medical records were retrieved for all patients whose most recent scans (either one or both eyes) revealed the presence of mirror artifacts, and a retrospective chart review was conducted of all cases. The following data were obtained from the medical records:

- Background demographic data, including age, sex, and ethnicity
- Snellen visual acuity (VA; converted to logMAR for statistical analysis)
- Retina, glaucoma, and/or neuro-ophthalmic diagnoses
- Spherical equivalent[24] (calculated as spherical cylinder/2); all spherical equivalents were calculated for eyes before cataract or refractive surgery
- Degree of myopia (modified from Grosvenor[25]): hyperopia (spherical equivalent > 0); emmetropia (spherical equivalent 0); mild myopia ($0 >$ spherical equivalent > -2.0); moderate myopia ($-6.0 <$ spherical equivalent ≤ -2.0); and high myopia (spherical equivalent ≤ -6.0)
- Lens status: presence of cataracts (defined as $\geq 2+$ nuclear sclerosis, or any subcapsular or cortical opacities), pseudophakia, or aphakia

Chart Review, No-Mirror-Artifacts Group

A subset of patients scanned with the macular cube 512 × 128 protocol were identified who had scans that did not exhibit mirror

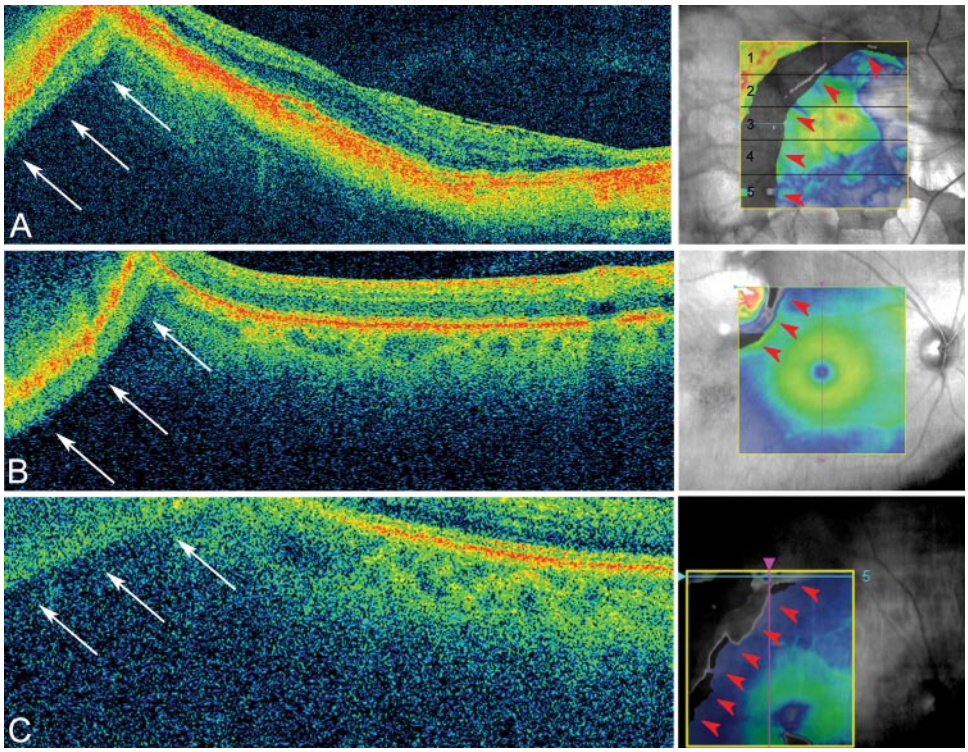

FIGURE 2. Causes of mirror artifacts (all scans acquired using Cirrus macular cube 512 × 128. (**A**) A mirror artifact generated in a patient with high myopia is seen at the *top left* corner of the scan (*arrows*, *left*). A crescent-shaped defect is observed on topographic map due to the segmentation breakdown caused by the mirror artifact. The defect occupies five of five of the regions on the macular map (*red arrowheads*, *right*). This scan correlates to the *light blue line* on the topographic map (raster 64). (**B**) A mirror artifact caused by the thickening or elevation of the retina. *Top left* (*arrows*): the scan has flipped onto itself due to the presence of a superotemporal choroidal nevi. A segmentation defect is seen at the *top left* (*red arrowheads*, *right*). The scan (raster 1) correlates to the *light blue line* on the topographic map. (**C**) This patient was only slightly myopic (−0.63 D), but visual acuity was poor (20/200). In this case, the cause of the mirror artifact was due to retinal disease (neovascular AMD), which caused poor visual acuity and led to eccentric fixation. A segmentation defect was seen at the *top left* of the macular map (*red arrowheads*, *right*). The scan (raster 5) correlates to the *light blue line* on the topographic map.

artifacts, and they served as control subjects. Because of the large volume of data, a random subset of patients was obtained to represent the overall population of scans without artifacts. The following equation was used to estimate an adequate sample size:

$$n = \frac{z^2 \cdot \hat{p} \cdot (1 - \hat{p})}{E^2}$$

where $z = 1.96$ (calculated with 95% confidence interval and $\alpha = 0.05$), $\hat{p} = 8.6\%$ (estimated percentage of patients with moderate to high myopia in the United States[26]; $E = 5\%$ (error). Under these assumptions, an adequate sample size was determined to be 121 patients. A random-number generator written in commercial software (MatLab; The MathWorks, Inc., Natick, MA) was created to select a group of 121 patients randomly from the patients without mirror artifacts. The same medical record review was completed for this group as for patients with mirror artifacts.

Statistical Analysis

Demographic Data. Demographic data for eyes with mirror artifacts were compared with data for eyes without artifacts. Two-tailed *t*-tests were used to determine statistical significance of age and visual acuity between the two groups, although statistical significance for sex, ethnicity, and lens status were determined via χ^2 tests (all statistical analyses, Excel; Microsoft Corp., Redmond, WA).

Spherical Equivalent, Degree of Myopia, and Severity of Mirror Artifacts. The overall prevalence of mirror artifacts was determined on a per-patient basis. The average spherical equivalent of eyes with mirror artifacts was compared with those without artifacts by two-tailed *t*-test. The spherical equivalent was also classified into subcategories (emmetropia, mild/moderate/high myopia, and hyperopia), and the groups were compared by χ^2 test.

Severity of the artifacts was calculated by dividing the topographic map into five regions. The following convention was used in the division of the 128-horizontal-raster-scan topographic map (from the superior to the inferior macula; Fig. 2A, right):

- Region 1 (25 scans: rasters 1–25)
- Region 2 (26 scans: rasters 26–51)
- Region 3 (central; 26 scans: rasters 52–77)
- Region 4 (26 scans: rasters 78–103)
- Region 5 (25 scan: rasters 104–128)

The scans were grouped according to the increasing number of regions of the map involved (from one of five to five of five), and then the average spherical equivalent and logMAR VA were calculated for each category. Analysis of variance (ANOVA) was used to evaluate differences in average spherical equivalent or VA, each grouped by the severity of mirror artifacts (one of five to five of five regions containing errors).

TABLE 1. Demographics Data

Variables	Mirror Artifacts (148 Patients, 200 Eyes)	No Mirror Artifacts (121 Patients, 121 Eyes)	*P*
Mean age ± SD	61 ± 13	66 ± 16	0.002*
Sex (*n*), males/females	87/61	63/58	0.430†
Ethnicity, *n* (%)			
Caucasian	112 (75.7)	92 (76.0)	0.510†
Asian	26 (17.6)	20 (16.5)	
African	7 (4.7)	3 (2.5)	
American other	3 (2.1)	6 (5.0)	
Diagnosis, *n*			
Suspected glaucoma	51	35	
POAG	39	32	
Other glaucoma	23	23	
Myopic degeneration	18	0	
Retinal detachment	9	1	
Retinal peripheral alterations	4	1	
Neovascular AMD/CNVM	11	7	
Vitreomacular interface diseases	9	6	
Non-neovascular AMD	7	4	
Macular hole	5	2	
Other maculopathy	2	3	
BRVO	3	0	
Diabetic retinopathy	1	3	
Choroidal nevi	2	1	
Optic disc drusen	1	2	
Retinal migraine	1	2	
Others‡	12	4	
Visual acuity, Snellen (logMAR)§	20/47 (0.37)	20/29 (0.16)	<0.001*
Lens status, *n* (%)			
No cataracts	110 (55.0)	69 (57.0)	0.002†
Cataracts	33 (16.5)	27 (22.0)	
Pseudophakia	49 (24.5)	24 (20.0)	
Aphakia	8 (4.0)	1 (1.0)	
Refractive surgery, *n*	5	0	0.060‖

Only 176/189 (93.1%) of patients had refraction data. CNVM, choroidal neovascular membrane; BRVO, branch-retinal vein occlusion.

* Two-tailed *t*-test.

† χ^2 test ($\alpha = 0.05$).

‡ Includes diagnoses that were found in only one normal patient or one patient with mirror artifact. Thirteen diagnoses were found for 12 different patients with mirror artifacts: branch retinal artery occlusion (BRAO), cystoid macular edema (CME), central retinal artery occlusion (CRAO), lamellar hole, hypotonic maculopathy, idiopathic juxtafoveal telangiectasia (IJT), ischemic optic neuropathy, idiopathic polyploidal choroidal vasculopathy (IPCV), Kearn-Sayer syndrome, pigment dispersion syndrome, pseudohole, retinopathy of prematurity (ROP), and solar retinopathy. Five diagnoses were given for four different normal patients: angioid streak, central serous chorioretinopathy (CSCR), diabetic macular edema, optic atrophy, and retinal ischemia.

§ 198/200 eyes with mirror artifacts had visual acuity data.

‖ Fisher's exact test.

RESULTS

Demographic Data

A total of 1592 patients seen at the New England Eye Center were scanned with the macular cube 512 × 128 scan protocol between January 2008 and February 2009. Of this population, 148 patients (200 eyes), or 9.3%, had scans with evidence of mirror artifacts.

Demographic characteristics of the two groups (with and without mirror artifacts) are described in Table 1. The distribution of the sexes and ethnicities were similar between the two groups. Patients with mirror artifacts (age, 61 ± 13 years) were significantly younger than those without artifacts (66 ± 16 years; $P = 0.002$). Both groups contained a wide array of ocular diseases, with glaucoma and suspected glaucoma being the most common diagnoses. Central visual acuity was better in patients without mirror artifacts (20/29) than in those with artifacts (20/47; $P < 0.0001$). Five patients in the mirror artifacts group had undergone refractive surgery, whereas none had undergone this procedure in the control group ($P = 0.04$).

Spherical Equivalent, Degree of Myopia, and Severity of Mirror Artifacts

In the 200 eyes with mirror artifacts, 186 (93.0%) had refractive data. The average spherical equivalent of the mirror artifact group was significantly more myopic (−4.54 ± 5.12 D) that that of the group without mirror artifacts (−0.12 ± 2.59 D; $P < 0.001$). Of the 121 randomly selected patients without artifacts, half (49.59%) were hyperopic. In the group with mirror artifacts, most of the spherical equivalents were found within the moderate (42.47%) to high (30.65%) myopia range ($P < 0.001$). In addition, a subgroup of 38 patients with axial length data was separated into those with and without mirror artifacts, and those with artifacts had significantly longer axial lengths (26.54 ± 2.84) than those without them (22.88 ± 1.01; $P = 0.004$).

The macular scan area was divided evenly into five regions, and artifact severity was grouped via the level of coverage on the topographic map, from one of five to five of five regions. Segmentation errors affecting two of five regions of the map contained the most individuals (61 patients), whereas errors affecting four of five regions of the map contained the fewest

TABLE 2. Spherical Equivalent, Degree of Myopia, and Severity of Mirror Artifacts

Variables	Mirror Artifacts (186/200 Eyes)	No Mirror Artifacts (121 Eyes)	*P*
Spherical equivalent, mean ± SD*	−4.54 ± 5.12	−0.12 ± 2.59	<0.001†
Myopia status, *n* (%)			
Emmetropia, SE = 0 D	11 (5.91)	13 (10.74)	
Mild myopia, SE < 0 to > −2.0 D	14 (7.53)	21 (17.36)	
Moderate myopia, SE = −2.0 to > −6.0 D	79 (42.47)	24 (19.83)	<0.001‡
High myopia, SE ≤ −6.0 D	57 (30.65)	3 (2.48)	
Hyperopia, SE > 0 D	25 (13.44)	60 (49.59)	
Artifact severity vs. SE, mean *n* ± SD			
1/5 regions	−3.87 ± 18.08 (34)	NA	
2/5 regions	−4.35 ± 30.84 (61)	NA	
3/5 regions	−4.30 ± 21.17 (23)	NA	0.730§
4/5 regions	−6.07 ± 9.31 (12)	NA	
5/5 regions	−4.91 ± 32.47 (56)	NA	
Artifact severity vs. VA, mean logMAR ± SD (Snellen)‖			
1/5 regions	0.26 ± 0.16 (20/37)	NA	
2/5 regions	0.28 ± 0.16 (20/38)	NA	
3/5 regions	0.38 ± 0.21 (20/48)	NA	0.040§
4/5 regions	0.41 ± 0.12 (20/51)	NA	
5/5 regions	0.51 ± 0.34 (20/65)	NA	

* 86/200 eyes with mirror artifacts have spherical equivalence data.
† Calculated using two-tailed *t*-test.
‡ Calculated using χ^2 test ($\alpha = 0.05$).
§ Calculated using analysis of variance.
‖ 198/200 eyes with mirror artifacts have visual acuity data.

(12 patients). The spherical equivalent for each group was calculated and the most myopic spherical equivalent was for scans covering four of five regions of the topographic map (−6.07 ± 9.31) and the least myopic spherical equivalent was for scans covering two of five regions of the map (−3.87 ± 18.08; $P = 0.73$). Artifact severity was also grouped and compared with visual acuity. There was a significant progressive trend ($P = 0.04$) with the better VA corresponding to smaller levels of breakdown (less artifact severity) and worse VA corresponding to higher levels of breakdown (high artifact severity). Average spherical equivalent, degree of myopia, and severity of mirror artifacts between eyes with and without mirror artifacts are compared in Table 2.

DISCUSSION

In this study we investigated mirror artifacts, which to our knowledge, have not yet been described in the clinical literature. Since it is an artifact of the Fourier-domain detection used in SD-OCT, it is not present in time-domain OCT (Fig. 3A).

In general, Cirrus HD-OCT is effective at capturing the details of the highly myopic eye that the StratusOCT (both Carl Zeiss Meditec, Inc.) often misses. The high scan speed of the SD-OCT extends retinal coverage and decreases motion artifacts. The improved resolution of the Cirrus HD-OCT from 10 to 5 μm also helps to delineate internal retinal structure in ocular disease. Since SD-OCT technology detects the interference spectrum and uses Fourier transformation to generate OCT images, it is interesting to note that this technology inherently produces mirror artifacts at the same time that it enables significant speed improvement. Although the Cirrus HD-OCT was the only device analyzed for the presence of mirror artifacts, all commercial SD-OCT instruments exhibit mirror artifacts. The prevalence of mirror artifacts is expected to be related to the axial measurement range of the instrument, with a smaller axial measurement range resulting in increased prevalence of artifacts.

Of all the patients imaged, 9.3% had scans containing mirror artifacts in one or both eyes. It is not only surprising that the prevalence of the artifact was so high, but it is also clinically important because mirror artifacts cause peripheral breakdown in segmentation (Fig. 2). It should be noted that the segmentation breakdown caused by this artifact primarily occurred in the periphery of the macular scans, because imaging was performed with the 0-delay line in front of the retina, and the retinal curvature can cause the peripheral retina to cross

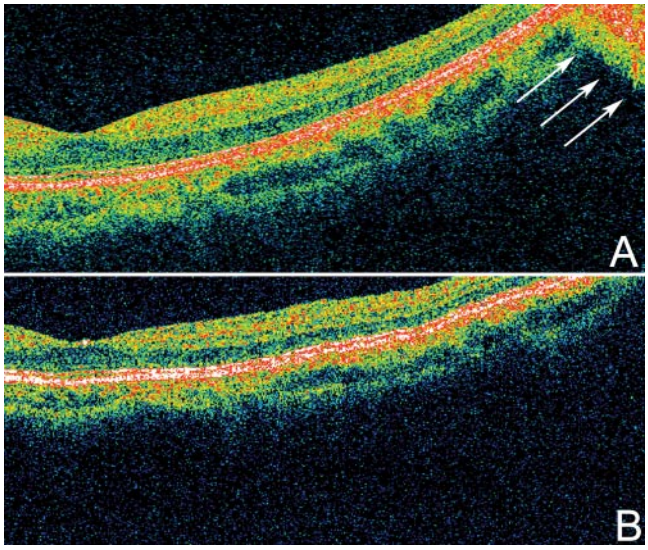

FIGURE 3. Time-domain versus SD-OCT in the generation of mirror artifacts. (**A**) Cirrus HD OCT five-line raster protocol with SD detection was used to acquire this scan from a patient with high myopia. The retina appeared tilted due to the long axial length of the eye. Mirror artifacts were observed in this scan (*arrows*). Individual retinal layers were better delineated with SD-OCT than with time-domain OCT. (**B**) StratusOCT with time-domain detection was used to acquire this scan from the same patient, by means of the macular thickness protocol. Although part of the retina crossed the 0-delay line (*top right*), no mirror artifact was observed.

the 0-delay line. Therefore, the central foveal region (the central 1 mm on the ETDRS map)—an area commonly used in making clinical treatment decisions—was rarely affected. However, highly myopic patients are at risk of various diseases, such as choroidal neovascular membranes, which may lead to the accumulation of intra- and subretinal fluids in center and peripheral regions of the macula. The dense scans obtainable with SD-OCT allow for accurate measurement of the volumes of various diseases, in the absence of segmentation errors. Thus, mirror artifacts may inhibit accurate quantitative OCT volumetric and thickness analysis, because investigators would not be able to accurately assess whether the decrease in retinal volume is due to treatment efficacy or to segmentation breakdown associated with mirror artifacts.

Visual acuity was worse in the patients with mirror artifacts (20/47) than in the ones without (20/29; $P = <0.001$). This finding is not surprising, since the patients with mirror artifacts on average had more myopic spherical equivalent (-4.54 ± 5.12 D) than did those without artifacts (-0.12 ± 2.59 D; $P < 0.001$). In addition, when the level of mirror artifacts was separated into five categories, there was a significant trend toward correlation of worse visual acuity with higher levels of breakdown ($P = 0.04$). However, when spherical equivalent from each segmentation breakdown level was compared, there was not a clear trend between the two variables ($P = 0.73$).

The patients with mirror artifacts had more myopic spherical equivalent on average than did the patients without artifacts ($P = 0.002$). In addition, the most common spherical equivalent classification in patients with mirror artifacts was moderate and high myopia, whereas in patients without mirror artifacts, it was hyperopia ($P < 0.001$). The low prevalence of hyperopic patients with mirror artifacts may be attributable to the short axial lengths of their eyes, which resulted in a flatter retina. In fact, subgroup analysis of the patients with axial length data demonstrated that those with mirror artifacts had longer axial lengths (26.54 ± 2.84) than did those without mirror artifacts (22.88 ± 1.01, $P = 0.004$). Some patients with mirror artifacts also had myopic degeneration ($n = 18$), whereas patients without the artifacts did not.

It makes intuitive sense that patients with higher myopia status would have higher prevalence of mirror artifacts, since the elongated axial length of the eye or the presence of posterior staphylomas predispose the periphery of the retina to cross the 0-delay line. This tendency is in contrast to eyes without myopia, where the periphery of the retina crosses at the nasal and temporal sides of the OCT scan region, away from the 0-delay line.

Although the majority (73.12%) of the patients with mirror artifacts were moderately to highly myopic, a subset (19.35%) of patients with artifacts was in fact emmetropic or hyperopic. In these cases, mirror artifacts could be the result of disease states causing mass thickening of the retina, such as neovascular age-related macular degeneration or retinal detachment (Fig. 2C). More important, mirror artifacts could be the result of poor positioning of the OCT scans, because of either placement too close to the 0-delay line or the extreme tilting of the scan that results when the OCT instrument is aligned with the scan beam off center in the pupil of the eye, causing the retina to cross the 0-delay line at the periphery. These factors are highly operator dependent, and it is therefore important to be aware of the potential consequences of poor scan positioning, to ensure proper scan placement in all patients.

The high prevalence of mirror artifacts and its potential clinical impact suggest that current designs of commercially available OCT devices are not sufficient for imaging moderately to highly myopic eyes. Several imaging system improvements are possible to mitigate or avoid this artifact. It is interesting to consider the possibility of increasing the axial scan depth range of OCT instruments to make it less likely for the retina to cross the 0-delay position and thus reduce the frequency of mirror artifacts. However, there is a tradeoff between the axial scan depth and the axial image resolution that arises from the limited number of pixels on the line scan camera that measures the interference spectrum. The number of pixels or resolvable elements in the axial direction is limited to the number of camera pixels divided by two. Most commercial OCT instruments are limited to 1024 axial pixels in the image. Increasing axial image resolution requires more axial pixels to visualize finer axial features and therefore decreases the axial scan depth range, making the frequency of mirror artifacts higher. Not all manufacturers explicitly specify the axial depth range; however, this factor is an important one to consider in an OCT instrument. Last, it is unclear why the average age of patients with mirror artifacts (61 ± 13 years) was younger than that of those without (66 ± 16). However, the age difference between the two groups (although significant, $P = 0.002$) was only 5 years and thus is not likely to be clinically significant.

There are several research techniques that enable the axial scan depth to be extended. A full-range, complex-conjugated SD-OCT could be devised by extracting or modulating the phase information of the OCT interferogram, such that one side of the symmetric SD-OCT scan is flipped to the other side.[14,16,17,20,21,23] However, current techniques for full-range imaging often require obtaining multiple scans, which reduces the effective scan rate. Makita et al.[23] presented a prototype spectral domain OCT with an extinction ratio exceeding 41 dB, which may be sufficient to eliminate mirror artifacts in most patients. Thus, this method may be used in future-generation commercial spectral-domain OCT devices to eliminate the high levels of mirror artifacts observed in patients with moderate to high myopia.

Limitations

Mirror artifacts caused a distinct pattern of segmentation line breakdown, appearing as a crescent-shaped defect on all 5×5-mm macular cube 512×128 maps (Fig. 2A, right). Although this crescent-shaped defect was clearly caused by mirror artifacts most of the time, there were a few instances in which the presence of the crescent did not clearly show mirror artifacts visually. In examining scans from both eyes of patients with mirror artifacts, we found that 10.8% of the eyes that demonstrated the crescent-shaped breakdown had no visible artifact. The presence of crescent defect in the absence of visible mirror artifacts was due to the artifacts' being too small and too far out in the periphery to be observed visually. Patients with crescent defects without visible mirror artifacts were not included in the 9.3% calculated overall prevalence, since in this study artifacts were defined in a clinical manner via visualization of OCT scans by observers.

We found that worse VA correlated with higher levels of mirror artifacts, perhaps because of the association between VA and the axial length of the eye. Although axial length is not a measurement performed on every patient seen at the Eye Center, a subgroup analysis of 38 patients with this measurement was conducted, and it showed that scans with mirror artifacts had significantly longer axial lengths compared with scans without mirror artifacts ($P = 0.004$). This finding supports the hypothesis that axial length is the prime factor in the generation of mirror artifacts. However, macular diseases may also negatively affect visual acuity, leading to poor central fixation, and so these are also probable contributing factors in the generation of mirror artifacts. In addition, future studies with more patients with axial length data should be conducted to further verify this association.

A variety of glaucomas and neuro-ophthalmic and retinal diseases were represented in the groups with and without

mirror artifacts. However, glaucoma and suspected glaucoma were the most common diagnoses in both groups. The high prevalence of glaucoma across both groups occurred because Cirrus HD-OCT is used as a baseline examination for all patients seen at the Glaucoma Service at the New England Eye Center. For retina and neuro-ophthalmology services, the Cirrus HD-OCT is currently an ancillary OCT test and is not yet used as a standard baseline test for all patients.

CONCLUSIONS

To our knowledge, this investigation is the first clinical study of the mirror artifact in spectral/Fourier-domain OCT. This image artifact is mainly associated with moderate to high myopic patients and is unique to Fourier-domain OCT. Our study was performed with the Cirrus OCT with an axial imaging depth range of 2 mm. Patients exhibiting mirror artifacts have significantly more myopic spherical equivalent ($P < 0.001$), VA ($P < 0.001$), longer axial lengths ($P = 0.004$), and higher proportions of moderate and high myopia compared with those without artifacts ($P < 0.001$). Increased severity of mirror artifacts is associated with worse VA ($P = 0.04$). Changes in hardware design may be necessary to reduce the frequency of mirror artifacts in moderately and highly myopic eyes. Larger axial imaging depth ranges are expected to reduce the frequency of mirror artifacts, and the axial imaging depth range is an important specification of an OCT instrument. In attempting to reduce the occurrence of mirror artifacts, operators should be advised to properly position the retina to avoid crossing the 0-delay line. In cases in which peripheral abnormalities in topographic measurements of retinal thickness are found, corresponding OCT scans should be examined for the presence of mirror artifacts.

References

1. Huang D, Swanson EA, Lin CP, et al. Optical coherence tomography. *Science.* 1991;254:1178–1181.
2. Srinivasan VJ, Adler DC, Chen Y, et al. Ultrahigh-speed optical coherence tomography for three-dimensional and en face imaging of the retina and optic nerve head. *Invest Ophthalmol Vis Sci.* 2008;49:5103–5110.
3. Potsaid B, Gorczynska I, Srinivasan VJ, et al. Ultrahigh speed spectral/Fourier domain OCT ophthalmic imaging at 70,000 to 312,500 axial scans per second. *Opt Express.* 2008;16:15149–15169.
4. Drexler W, Fujimoto JG. State-of-the-art retinal optical coherence tomography. *Prog Retin Eye Res.* 2008;27:45–88.
5. Wojtkowski M, Srinivasan V, Fujimoto JG, et al. Three-dimensional retinal imaging with high-speed ultrahigh-resolution optical coherence tomography. *Ophthalmology.* 2005;112:1734–1746.
6. Kaiser PK, Blodi BA, Shapiro H, Acharya NR. Angiographic and optical coherence tomographic results of the MARINA study of ranibizumab in neovascular age-related macular degeneration. *Ophthalmology.* 2007;114:1868–1875.
7. Konno S, Akiba J, Yoshida A. Retinal thickness measurements with optical coherence tomography and the scanning retinal thickness analyzer. *Retina.* 2001;21:57–61.
8. Ray R, Stinnett SS, Jaffe GJ. Evaluation of image artifact produced by optical coherence tomography of retinal pathology. *Am J Ophthalmol.* 2005;139:18–29.
9. Krebs I, Falkner-Radler C, Hagen S, et al. Quality of the threshold algorithm in age-related macular degeneration: Stratus versus Cirrus OCT. *Invest Ophthalmol Vis Sci.* 2009;50:995–1000.
10. Patel PJ, Chen FK, da Cruz L, Tufail A. Segmentation error in Stratus optical coherence tomography for neovascular age-related macular degeneration. *Invest Ophthalmol Vis Sci.* 2009;50:399–404.
11. Sadda SR, Wu Z, Walsh AC, et al. Errors in retinal thickness measurements obtained by optical coherence tomography. *Ophthalmology.* 2006;113:285–293.
12. Leung CK, Chan WM, Chong KK, et al. Alignment artifacts in optical coherence tomography analyzed images. *Ophthalmology.* 2007;114:263–270.
13. Wojtkowski M, Leitgeb R, Kowalczyk A, et al. In vivo human retinal imaging by Fourier domain optical coherence tomography. *J Biomed Opt.* 2002;7:457–463.
14. Wojtkowski M, Kowalczyk A, Leitgeb R, Fercher AF. Full range complex spectral optical coherence tomography technique in eye imaging. *Opt Lett.* 2002;27:1415–1417.
15. Hofer B, Povazay B, Hermann B, et al. Dispersion encoded full range frequency domain optical coherence tomography. *Opt Express.* 2009;17:7–24.
16. Choma MA, Yang C, Izatt JA. Instantaneous quadrature low-coherence interferometry with 3 x 3 fiber-optic couplers. *Opt Lett.* 2003;28:2162–2164.
17. Vakoc BJ, Yun SH, Tearney GJ, Bouma BE. Elimination of depth degeneracy in optical frequency-domain imaging through polarization-based optical demodulation. *Opt Lett.* 2006;31:362–364.
18. Yun S, Tearney G, de Boer J, Bouma B. Removing the depth-degeneracy in optical frequency domain imaging with frequency shifting. *Opt Express.* 2004;12:4822–4828.
19. Motaghian Nezam SM, Vakoc BJ, Desjardins AE, et al. Increased ranging depth in optical frequency domain imaging by frequency encoding. *Opt Lett.* 2007;32:2768–2770.
20. Leitgeb RA, Hitzenberger CK, Fercher AF, Bajraszewski T. Phase-shifting algorithm to achieve high-speed long-depth-range probing by frequency-domain optical coherence tomography. *Opt Lett.* 2003;28:2201–2203.
21. Yasuno Y, Makita S, Endo T, et al. Simultaneous B-M-mode scanning method for real-time full-range Fourier domain optical coherence tomography. *Appl Opt.* 2006;45:1861–1865.
22. Wang RK. In vivo full range complex Fourier domain optical coherence tomography. *Appl Phys Lett.* 2007;90:054103.
23. Makita S, Fabritius T, Yasuno Y. Full-range, high-speed, high-resolution 1 micron spectral-domain optical coherence tomography BM-scan for volumetric imaging of the human posterior eye. *Opt Express.* 2008;16:8406–8420.
24. Luo HD, Gazzard G, Liang Y, et al. Defining myopia using refractive error and uncorrected logMAR visual acuity >0.3 from 1334 Singapore school children ages 7–9 years. *Br J Ophthalmol.* 2006;90:362–366.
25. Grosvenor T. A review and a suggested classification system for myopia on the basis of age-related prevalence and age of onset. *Am J Optom Physiol Opt.* 1987;64(7):545–554.
26. Sperduto RD, Seigel D, Roberts J, Rowland M. Prevalence of myopia in the United States. *Arch Ophthalmol.* 1983;101:405–407.